Title
Rare-Earth Disilicate-Silicon Nitride Ceramics: II. Oxidation Behavior

Journal
Journal of the American Ceramic Society, 75(8)

Authors
Cinibulk, M.K.
Thomas, G.
Johnson, S.M.

Publication Date
1991-11-01

LBL-31454
Preprint

Lawrence Berkeley Laboratory
UNIVERSITY OF CALIFORNIA

Materials & Chemical Sciences Division

Submitted to the Journal of the American Ceramic Society

Rare-Earth Disilicate–Silicon Nitride Ceramics: II. Oxidation Behavior

M.K. Cinibulk, G. Thomas, and S.M. Johnson

November 1991

Prepared for the U.S. Department of Energy under Contract Number DE-AC03-76SF00098

DISCLAIMER

DISCLAIMER

LBL-31454

Rare-Earth Disilicate–Silicon Nitride Ceramics: II. Oxidation Behavior

Michael K. Cinibulk[#*] and Gareth Thomas[#]

Department of Materials Science and Mineral Engineering
University of California
and
Center for Advanced Materials
Materials Sciences Division
Lawrence Berkeley Laboratory
University of California
Berkeley, California 94720

Sylvia M. Johnson[#]

Materials Research Laboratory
SRI International
Menlo Park, CA 94025

November 1991

[#]Member, American Ceramic Society
[*]Currently with Max-Planck-Institut für Metallforschung, Stuttgart, FRG

This work was supported in part by the National Science Foundation under Contract No. DMR 83-1317239 and by the Director, Office of Energy Research, Office of Basic Energy Sciences, Materials Sciences Division, of the U.S. Department of Energy under Contract No. DE-AC03-76SF00098.

Abstract

The oxidation behavior and microstructure of the oxidized surfaces of $RE_2Si_2O_7$-Si_3N_4 ceramics were investigated. The high oxidation resistance of these materials at 1400°C is attributed to the minimization of amorphous phases via devitrification to disilicates that are in equilibrium with SiO_2, the oxidation product of Si_3N_4. Crystals of $RE_2Si_2O_7$ grew out of the surface silicate in preferred orientations that were dictated by crystal structure. The morphology of the microstructure of the oxidized surfaces was shown to be partially dependent on the concentration of impurities; the presence of Ca was found to coincide with the growth of $Gd_2Si_2O_7$ and $Dy_2Si_2O_7$ crystals with high aspect ratios. [Key Words: intergranular phase, microstructure, oxidation, rare-earth oxides, silicon nitride.]

I. Introduction

Silicon nitride ceramics are among the most promising materials for use as structural components in high-temperature oxidizing environments. However, Si_3N_4 is difficult to sinter to theoretical density without the use of additives that form a eutectic liquid through which mass transport, and hence densification, is enhanced. It is this liquid that forms the intergranular phase in Si_3N_4 ceramics, on which the high-temperature behavior depends. Few studies have discussed the oxidation behavior of Si_3N_4 sintered with oxides of the lanthanide metals.[1-4] In these investigations Si_3N_4 sintered with only the lighter, less refractory lanthanides (La, Ce, and Sm) was studied. The oxidation resistance of Y_2O_3-sintered Si_3N_4 has been found to be superior to that of the other RE_2O_3-sintered Si_3N_4 materials.[4]

The design, fabrication, and microstructural characterization of RE_2O_3-sintered Si_3N_4 ceramics tailored specifically for high temperatures has been previously described.[5] Lange et al.[6] have shown that in the Si_3N_4-SiO_2-Y_2O_3 system, $Y_2Si_2O_7$ is the most

oxidation resistant secondary phase for Si_3N_4 ceramics because it is the only Y-containing phase in equilibrium with SiO_2, the oxidation product of Si_3N_4. The disilicates of the lanthanides should also be stable toward oxidation since phase relations in the Si_3N_4-SiO_2-RE_2O_3 systems are generally considered to be analogous to those in the Si_3N_4-SiO_2-Y_2O_3 system.[7-9] The crystallization behavior of all six disilicates as the secondary phases was similar, characterized by a limited nucleation and rapid growth mechanism resulting in large single crystals. Complete crystallization of the intergranular phase was obtained with the exception of a thin residual amorphous film which was observed at interfaces and believed to be rich in impurities, the cause of incomplete devitrification. In this paper the oxidation behavior and the microstructure of the oxidized surfaces of these $RE_2Si_2O_7$-Si_3N_4 materials is discussed.

II. Experimental Procedure

(1) Material

The sintered Si_3N_4† ceramics were prepared with a 2:1 molar ratio of SiO_2:RE_2O_3 (taking into account oxide present on the surface of Si_3N_4 particles), placing the composition directly on the Si_3N_4-$RE_2Si_2O_7$ tie line.[5] These materials contain a 12.3 vol% grain-boundary phase; this volume fraction is equivalent to a 15 wt% $Y_2Si_2O_7$-Si_3N_4 material, which was found to sinter to >99 % theoretical density. The materials were subjected to a heat-treatment at 1400°C for 24 hr to crystallize the secondary $RE_2Si_2O_7$ phase. X-ray diffraction and electron microscopy confirmed a completely crystalline secondary phase with a thin (1-10 nm) residual amorphous film at all two-grain boundaries for all materials with the exception of the $Yb_2Si_2O_7$-Si_3N_4 material. The $Yb_2Si_2O_7$-Si_3N_4 material had isolated regions with incompletely devitrified multiple-grain junctions, which were attributable to compositional heterogeneities in the powder compact during processing.

(2) Oxidation

Oxidation studies were conducted at 1400°C over a period of ~200 hr in laboratory air. Samples 3 mm x 4 mm x 45 mm were cut from the sintered blocks. The surfaces were ground with a 320 grit diamond wheel, then polished to a 15 μm finish. Prior to oxidation, the surfaces were ultrasonically cleaned in acetone followed by a cleaning in ethanol. The specimens, on platinum wire supports in an alumina tray, were placed in a high-temperature box furnace at 400°C and heated to 1400°C within 15 min. The furnace was cooled to 400°C and the specimens removed at 12-48 hr intervals for weighing on an analytical balance having microgram resolution to determine weight change as a function of time. The materials were characterized by x-ray diffraction to identify crystalline phases present on the surfaces of the oxidized ceramics, which were scanned using Cu Kα radiation. The oxidized surfaces then were characterized by scanning electron microscopy and energy-dispersive x-ray spectroscopy.

III. Results

(1) Oxidation Kinetics

Fig. 1 is a plot of weight gain per unit surface area as a function of time at 1400°C. All materials had specific weight gains on the order of 0.25-0.35 mg/cm^2 after 192 hr with the exception of the $Sm_2Si_2O_7$-Si_3N_4 material which had a weight gain of 0.64 mg/cm^2 after the same time at temperature. The oxidation of sintered silicon nitride has been shown to obey a parabolic-type of rate law such that

$$W^2 = kt$$

were W is the weight gain per unit surface area, k is the parabolic oxidation rate constant, and t is exposure time.[10] Plotting these data parabolically results in straight lines for all curves but those for the $Sm_2Si_2O_7$-Si_3N_4 and $Dy_2Si_2O_7$-Si_3N_4 materials, as shown in

Fig. 2. The $Dy_2Si_2O_7$-Si_3N_4 material deviates only slightly while $Sm_2Si_2O_7$-Si_3N_4 departs significantly from linearity when plotted parabolically. The oxidation resistance of these materials can be correlated reasonably well with the refractoriness of the RE_2O_3-SiO_2 system, i.e. inversely related to the eutectic temperature in each system. These temperatures are listed in Table 1. The $Y_2Si_2O_7$-Si_3N_4 material fell in the middle of the group with respect to oxidation resistance while the $Er_2Si_2O_7$-Si_3N_4 material displayed the best resistance toward oxidation.

Table I contains the parabolic oxidation rate constants for the six compositions investigated, as well as the total specific weight gain after 192 hr. The parabolic oxidation behavior of these ceramics indicates a diffusional process as the rate-limiting step in the oxidation mechanism, associated with the migration of additive (RE^{3+}) and impurity cations along residual amorphous grain-boundary phases to the interface between ceramic and the surface oxide. The high oxidation resistance of these materials can be attributed to the presence of a minimal amount of amorphous grain-boundary phase, but with high viscosity due to the presence of refractory RE^{3+}, and the presence of thermodynamically stable crystalline secondary phases, such that the driving force for additive cation diffusion to the surface is minimized.

(2) Microstructure of Oxidized Surfaces

The phases identified by x-ray diffraction composing the oxidized surfaces of the six materials are summarized in Table 3. X-ray diffraction patterns of the oxidized surfaces identified α-cristobalite and the rare-earth disilicates to be the only major crystalline phases present. The disilicates crystallized on the surfaces into the same polymorphs as originally present as the secondary phase.[5] Also present were trace amounts of β-Si_3N_4 and Si_2ON_2. The β-Si_3N_4 peaks were smallest for those materials having the thickest oxide layers, indicating those signals were from the bulk ceramic beneath the oxidized surface layer. Spalling of the oxide from the substrate surfaces was not observed for any material.

SEM observations revealed the presence of two distinct morphologies for the rare-earth disilicates, a needle-like and a more equiaxed type. The oxidized surfaces also contained an amorphous silicate phase, from which cristobalite and $RE_2Si_2O_7$ grains crystallized as shown in Figs. 3 and 4. Fig. 4 was obtained using backscattered electrons to gain contrast differences, strongly dependent on composition. In each image the darkest phase in the background is cristobalite, the intermediate phase surrounding the cristobalite grains is the residual amorphous silicate phase, and the phase in brightest contrast growing out of the silicate phase is the rare-earth disilicate. The dark jagged lines traversing the surfaces are cracks associated with either differential thermal expansion between the bulk and oxide layers or with the volumetric change accompanying transformation of surface cristobalite from the β- to α-phase upon cooling.

The $Y_2Si_2O_7$ crystals appear to have grown much larger in size than any of the other rare-earth disilicates and in a flattened elongated morphology The x-ray diffraction patterns of the six materials indicated the disilicates crystallized in preferred orientations, with the [0 0 1] direction normal to the surface for those disilicates with tetragonal (A-phase) and orthorhombic (δ-phase) crystal structures, and the [0 1 1] direction normal to the surface for those disilicates with monoclinic (β-phase) and triclinic (α-phase) structures. A similar behavior of growth of $Y_2Si_2O_7$ during oxidation has been reported by Babini et al.[11] with growth along the (1 1 0) plane and aligned parallel to the oxide surface. They found texturing of the $Y_2Si_2O_7$ crystals to increase with temperature.-

While the oxidized surface of the $Y_2Si_2O_7$-Si_3N_4 ceramic consisted exclusively of flattened and elongated β-$Y_2Si_2O_7$ crystals, the oxidized surfaces of the $Sm_2Si_2O_7$-Si_3N_4, $Er_2Si_2O_7$-Si_3N_4, and $Yb_2Si_2O_7$-Si_3N_4 ceramics consisted exclusively of the respective disilicates in the equiaxed morphology. The oxidized surfaces of both the $Gd_2Si_2O_7$-Si_3N_4 and $Dy_2Si_2O_7$-Si_3N_4 ceramics contained disilicates of a needle-like morphology, but the equiaxed form still predominated. Becasue the needle-like morphology was observed only for disilicates having the orthorhombic structure, this

growth may be dependent on crystal structure. Energy dispersive x-ray spectroscopy of the disilicates indicated the presence of ~6-8 at.% Ca (as an impurity) associated with crystals having a whisker morphology while no appreciable Ca was detected in the equiaxed crystals. The cristobalite grains were found to be essentially free of impurities with less than 0.5 at.% Ca detected in the grains of all the materials. The remaining amorphous silicate phase surrounding the cristobalite grains had very high concentrations of impurity elements (~3-6 at.% each of Mg, Al, and Ca); these impurities are believed to have segregated to the grain-boundary phase from the Si_3N_4 and SiO_2 powders during sintering and then migrated to the surface during oxidation. Interestingly, this silicate phase was free from any but a trace amount of Fe.

IV. Discussion

(1) Oxidation Mechanism and Kinetics

The parabolic oxidation kinetics exhibited by sintered silicon nitride ceramics were originally assumed to be the result of a protective surface layer of SiO_2, as in the case of pure Si_3N_4. However, high-temperature exposure of silicon nitride sintered with oxide additives leads to accelerated oxidation attributable to the enhanced oxidation of Si_3N_4 dissolved in a highly viscous silicate phase present at the surface.[10] The work of Singhal[10] and Cubicciotti et al.[12,13] showed that the outward diffusion of additive cations (Mg^{2+} or Y^{3+}, as well as impurities of Al^{3+}, Ca^{2+}, and Fe^{3+}) and nitrogen, produced by the amorphous intergranular-phase/oxide-layer diffusion couple, and the inward diffusion of oxygen resulted in a compositional gradient beneath the oxide layer. Therefore, the parabolic oxidation kinetics exhibited by sintered Si_3N_4 ceramics is produced, not by a protective surface oxide layer, but by a compositional gradient lying beneath the oxidized surface layer.

The processed microstructures of these materials contained a thin residual amorphous film at all grain boundaries. Also, incomplete crystallization of the multi-grain junctions was observed in an isolated region of the $Yb_2Si_2O_7$-Si_3N_4 material prepared for

transmission electron microscopy. The presence of residual amorphous grain-boundary phases, which are never in equilibrium with SiO_2 (the oxidation product of Si_3N_4), result in the creation of a driving force for additive and impurity cation diffusion to the Si_3N_4-bulk/oxide-layer interface. Impurities such as Mg, Al, Ca, and Fe are known to segregate to the amorphous intergranular phase during liquid-phase sintering. The presence of these impurities in addition to the additive cations (RE^{3+}) determine to a great extent the properties of the amorphous phase.

In the materials studied, the secondary phases obtained are stable toward oxidation, therefore, the oxidation behavior was dependent solely on the amorphous intergranular-phase composition and the diffusion of its components to the bulk/oxide interface. The impurity content of the oxidized surfaces of all six materials was very similar, implying the differences obtained in oxidation behavior can be attributed to the effect of the additive cation (RE^{3+}) on amorphous-phase viscosity. The oxidation resistance of these materials is related to the eutectic temperatures of the respective RE_2O_3-SiO_2 binary systems; i.e., in the binary systems with the highest eutectic temperatures, the materials sintered with these additives generally have shown the lowest weight gains. For these chemically similar grain-boundary phases, the viscosities are, therefore, assumed to be related to the eutectic temperatures. Although the amorphous phase contains N (which is estimated to lower the eutectic temperature of the Y_2O_3-SiO_2 system by ~140°C, however raise its viscosity[14]), as well as the impurities mentioned, the effect of these constituents should be similar for all materials based on their similar compositions.

The one material which displayed greatly differing oxidation behavior was the $Sm_2Si_2O_7$-Si_3N_4 material. Whereas all other materials displayed, for the most part, parabolic oxidation kinetics, the $Sm_2Si_2O_7$-Si_3N_4 material deviated from this behavior and exhibited twice the weight gain as the other materials after 192 hr. Mieskowski and Sanders[4] also reported nearly twice the weight gain of a Sm_2O_3-sintered Si_3N_4 material as that of a Y_2O_3-sintered Si_3N_4 after 200 hr at 1370°C, however, they also reported parabolic

oxidation kinetics for both materials. Both materials were characterized as having completely amorphous grain-boundary phases.

The rate of weight gain of the $Sm_2Si_2O_7$-Si_3N_4 material in the present study was very high at first and then decreased to a rate similar to that of the other five materials. The apparent departure of the oxidation behavior from that of parabolic may involve a reduction in surface area as oxidation progresses by the sealing of open porosity by the oxidation product, with the net effect being a steady increase in specific weight (assuming a constant surface area). The $Sm_2Si_2O_7$-Si_3N_4 material had the lowest density (98%) of the six materials and therefore the existence of open porosity was likely. The increased surface area provided by porosity open to the surface initially would produce artificially high oxidation rates when calculating a surface area based on specimen dimensions alone. As oxidation proceeded and the pores were closed by oxidation product, this additional surface where reaction initially occurred would no longer be a source of reactant and the measured specific weight gain would approach the true weight gain per unit surface area as given by specimen geometry. Hence, following an initial period of oxidation where available surface area is continuously decreasing, the surface area becomes constant and parabolic oxidation kinetics are observed (Fig. 2).

The much higher apparent diffusivity of Sm cations through the grain-boundary phase than that of the other rare-earth cations cannot be explained on the basis of differences in eutectic temperatures of the systems alone. Although, the high specific weight gains initially occuring may be due to inaccurate estimates of surface area due to the presence of porosity, an additional explanation for the high rate of oxidation throughout the test may reside in the fact that Sm can exist in both the divalent and trivalent states.[15] Cerium can also exist in more than just the trivalent oxidation state. In CeO_2-sintered Si_3N_4 ceramics, CeO_2 is known to reduce to Ce_2O_3 during sintering under inert conditions according to the reaction[1,16]

$$12\ CeO_2 + Si_3N_4 = 6\ Ce_2O_3 + 3\ SiO_2 + 2\ N_2$$

The mechanism proposed[17] for the oxidation of CeO_2-sintered Si_3N_4 ceramics, involves the migration of Ce^{3+} cations from the grain-boundary phase to the bulk/oxide interface and subsequent dissolution in the amorphous surface silicate phase up to the equilibrium saturation, with excess Ce^{3+} being oxidized to Ce^{4+} by oxygen dissolved in the silicate resulting in the exolution of CeO_2 crystals. Si_3N_4 then dissolves in the silicate phase and reacts with the dissolved oxygen forming SiO_2 and the evolution of N_2.

A similar reduction/oxidation reaction is proposed for Sm in $Sm_2Si_2O_7$-Si_3N_4 ceramics. Although the trivalent state is the characteristic one for all lanthanides and they can all exist in the divalent state under unusual conditions, only Sm, Eu, and Yb have significant "normal" chemistry in the divalent state.[15] Atypical oxidation states are most prevalent for lanthanides when the ion can have empty, half-filled, or filled *f*-shells. Analogous to the reaction involving the reduction of CeO_2 to Ce_2O_3, samarium could exist as Sm^{2+} after reduction by dissolved nitrogen in the residual amorphous grain-boundary phase, which is known to be an oxynitride glass. The diffusion rate of divalent Sm is expected to be much greater than that of trivalent Sm,[15] which would account for the much greater weight gain upon oxidation of this material as compared with the weight gain of the other five materials. Upon reaching the bulk/oxide interface Sm^{2+} dissolves in the surface silicate phase and is subsequently oxidized to Sm^{3+}, reacts with dissolved SiO_2, and precipitates out of solution as $Sm_2Si_2O_7$. A problem with this hypothesis is that Yb can also exist in the divalent state, and as the observed oxidation kinetics of the $Yb_2Si_2O_7$-Si_3N_4 material are similar tothose of the other four materials, there is no reason to suspect the reduction of Yb^{3+} to Yb^{2+}.

(2). Morphology of Oxidized Surfaces

During the oxidation of sintered Si_3N_4 materials, the surface silica produced as the oxidation product of Si_3N_4 is brought to chemical equilibrium with those intergranular

phases not already existing in equilibrium with SiO_2 (amorphous phase and incompatible crystalline phases) by the outward diffusion of additive and impurity cations. The equilibrium condition changes as oxidation proceeds and the grain-boundary phase becomes depleted of these cations. Precipitation of crystalline $RE_2Si_2O_7$ and SiO_2 from the surface silicate melt maintains chemical equilibrium with the changing grain-boundary phase composition. The growth of crystals in preferred directions can be explained in terms of relative entropy changes as associated with growth.[17] A large ΔS results in the growth of faceted crystals due to anisotropic growth rates. A small ΔS results in the growth of isotropic crystals due to low growth-rate anisotropy. A large ΔS is expected for the growth of most inorganic compounds from the vapor phase or dilute solutions, including silicates from melts whereas a small ΔS accompanies the growth of most metals and SiO_2 from melts.[17] Figs. 3 and 4 indicate the isotropic growth of SiO_2 and the faceted growth of the disilicates as predicted by differences in changes in entropy of crystal growth.

Previous investigations[4,11] have reported the growth of $RE_2Si_2O_7$ crystals on the surface of the oxidized samples to be primarily in the form of needles and platelets. Babini et al.[11] have studied the effects of relative amounts of impurities in Y_2O_3/SiO_2-sintered Si_3N_4 on the evolution of the morphology of the oxidized surfaces. They concluded that viscosity of the surface silicate phase, ionic mobility and degree of oversaturation of the diffusing cations in the surface silicate were closely related to the rate of oxidation, and that the morphology of the $Y_2Si_2O_7$ crystallized in the oxidized surface was dependent on oxidation temperature, quenching rate, and ratio of impurities to Y^{3+} in the surface silicate.

All materials in the present investigation were oxidized under the same conditions (1400°C for ~200 hr) and according to the results of x-ray microanalysis, impurity concentrations in the oxidized surface layers of all six materials were about the same. The surfaces of all materials with the exception of the $Y_2Si_2O_7$-Si_3N_4 material contained $RE_2Si_2O_7$ crystals of equiaxed morphology, with that of $Y_2Si_2O_7$ being elongated and

plate-like. Only the $Gd_2Si_2O_7$-Si_3N_4 and $Dy_2Si_2O_7$-Si_3N_4 materials contained disilicates of the needle-like morphology and in both cases the needles contained ~6 at.% Ca, while the same disilicates in the equiaxed morphology did not. It is likely that Ca acts to catalyze the growth of these crystals along preferred planes to form high aspect ratios resulting from highly anisotropic growth rates. By sintering Si_3N_4 with the addition of a small amount of a dopant such as CaO, highly elongated β-Si_3N_4 grains have been known to be catalyzed,[18] resulting in a microstructure that exhibits improved fracture toughness. Such a mechanism may be responsible for the formation of the needle-like δ-$Gd_2Si_2O_7$ and δ-$Dy_2Si_2O_7$ grains in the presence of high Ca concentrations.

The needle-like morphology was only assumed by the disilicates which have orthorhombic crystal structures. The β-$Er_2Si_2O_7$ and β-$Yb_2Si_2O_7$ forming the equiaxed, granular-like crystals are monoclinic as is $Y_2Si_2O_7$ forming the flattened elongated crystals. The polymorphs of $RE_2Si_2O_7$ observed by others[4,11] to grow into needle-like crystals were not identified, however the oxidation temperatures of ~1300-1400°C suggest that the same polymorphs identified in the present study should have been present. The tetragonal structure of *A*-$Sm_2Si_2O_7$ resulted in highly faceted crystals, not unlike those of the orthorhombic δ-$Gd_2Si_2O_7$ and δ-$Dy_2Si_2O_7$.

V. Conclusions

(1) The resistance to oxidation of these materials was about an order of magnitude better than that of other sintered Si_3N_4 reported in the literature. The high oxidation resistance is attributed to the minimization of amorphous phases via devitrification to disilicates that are compatible with SiO_2, the oxidation product of Si_3N_4.

(2) The relative rates of oxidation found to be roughly inversely related to eutectic temperature of the SiO_2-RE_2O_3 system, indicating that a lower viscosity residual amorphous phase results in a higher rate of oxidation as the rate-limiting step is diffusion of additive and impurity cations through this amorphous phase to the oxidized surface. The

oxidation behavior displayed by these materials was parabolic, which is consistent with previous studies which indicated that parabolic kinetics prevail during the oxidation of Si_3N_4 ceramics.

(3) The oxidation of $Sm_2Si_2O_7$-Si_3N_4 and $Dy_2Si_2O_7$-Si_3N_4 was not found to display parabolic oxidation kinetics until after a certain exposure time. It is believed that the initially higher specific weight gains were obtained due to the presence of open porosity that was eventually sealed, leading subsequently to oxidation kinetics that were parabolic. The much higher oxidation rate of $Sm_2Si_2O_7$-Si_3N_4, even after sealing of porosity, could be due to the divalent nature of Sm in certain reducing environments, which would lead to enhanced transport to the oxidized surface.

(4) During oxidation $RE_2Si_2O_7$ grew out of the surface silicate in preferred orientations that were dictated by crystal structure. The morphology of the microstructure of the oxidized surfaces was shown to be partially dependent on the concentration of impurities; the presence of Ca was found to coincide with the preferred growth of $Gd_2Si_2O_7$ and $Dy_2Si_2O_7$ into needle-like whiskers.

† SN E-10, Ube Industries, Tokyo, Japan

Based on the dissertation submitted by M.K. Cinibulk for the Ph.D. degree in Materials Science and Engineering, University of California, Berkeley, CA 94720

Presented in part at the 93rd Annual Meeting of the American Ceramic Society, Cincinnati, OH, April 30, 1991 (Symposium Paper No. 25-SII-91).

Initially supported by the National Science Foundation under Contract No. DMR 83-1317239. Additional support was provided by the Director, Office of Energy Research, Office of Basic Energy Sciences, Materials Sciences Division of the U.S. Department of

Energy under Contract No. DE-AC03-76SF00098. Additional facilities were provided by SRI International.

References

1. F.F. Lange, "Si_3N_4-Ce_2O_3-SiO_2 Materials: Phase Relations and Strength," Am. Ceram. Soc. Bull., **59** [2] 239-40, 49 (1980).

2. C.L. Quakenbush and J.T. Smith, "Phase Effects in Si_3N_4 Containing Y_2O_3 or CeO_2: II, Oxidation," Am. Ceram. Soc. Bull., **59** [5] 533-37 (1980).

3. G.N. Babini, A. Bellosi, and P. Vincenzini, "Oxidation of Silicon Nitride Hot-Pressed with Ceria," J. Am. Ceram. Soc., **64** [10] 578-84 (1981).

4. D.M. Mieskowski and W.A. Sanders, "Oxidation of Silicon Nitride Sintered with Rare-Earth Oxide Additions," J. Am. Ceram. Soc., **68** [7] C-160-63 (1985).

5. M.K. Cinibulk, G. Thomas, and S.M. Johnson, "$RE_2Si_2O_7$-Si_3N_4 Ceramics: I, Design, Fabrication, and Secondary-Phase Crystallization ," J. Am. Ceram. Soc., this issue, (1992).

6. F.F. Lange, S.C. Singhal, and R.C. Kuznicki, "Phase Relations and Stability Studies in the Si_3N_4-SiO_2-Y_2O_3 Pseudoternary System," J. Am. Ceram. Soc., **60** [5-6] 249-52 (1977).

7. J. Ito and H. Johnson, "Synthesis and Study of Yttrialite," Am. Minerologist, **53** 1940-52 (1968).

8. J. Felsche, "Polymorphism and Crystal Data of the Rare-Earth Disilicates of the Type $RE_2Si_2O_7$," J. Less-Common Metals, **21** 1-14 (1970).

9. R.R. Wills, R.W. Stewart, J.A. Cunningham, and J.M. Wimmer, "The Silicon Lanthanide Oxynitrides," J. Mater. Sci., **11** 749-59 (1976).

10. S.C. Singhal, "Thermodynamics and Kinetics of Oxidation of Hot-Pressed Silicon Nitride," J. Mater. Sci., **11** 500-09 (1976).

11. G.N. Babini, A. Bellosi, and P. Vincenzini, "Factors Influencing Structural Evolution in the Oxide of Hot-Pressed Si_3N_4-Y_2O_3-SiO_2 Materials," J. Mater. Sci., **19** 3487-97 (1984).

12. D. Cubicciotti, K.H. Lau, and R.L. Jones, "Rate-Controlling Process in the Oxidation of Hot-Pressed Silicon Nitride," J. Electrochem. Soc., **124** [12] 1955-56 (1977).

13. D. Cubicciotti and K.H. Lau, "Kinetics of Oxidation of Hot-Pressed Silicon Nitride Containing Magnesia," J. Am. Ceram. Soc., **61** [11-12] 512-17 (1978).

14. R.A.L. Drew, S. Hampshire, and K.H. Jack, "Nitrogen Glasses," Proc. Br. Ceram. Soc., **31** 119-32 (1981).

15. F.A. Cotton and G. Wilkinson, Advanced Inorganic Chemistry, 5th Edition, Wiley-Interscience, New York, 1988.

16. J. Felsche and W. Hersiger, "Polymorphs of the Rare-Earth Pyrosilicates $RE_2Si_2O_7$-[RE: La, Ce, Pr, Nd, Sm]," J. Less-Common Metals, **18** [2] 131-37 (1969).

17. W.D. Kingery, H.K. Bowen, and U.R. Uhlmann, Introduction to Ceramics, 2nd Edition, Wiley-Interscience, New York, 1976.

18. A.J. Pyzik and D.R. Beamon, "Processing, Microstructure, and Properties of Self-Reinforced Silicon Nitride," presented at 92nd Ann. Meeting Am. Ceram. Soc., Dallas, TX, April 22-26, 1990.

Table 1. Oxidation Kinetics

Material	Rate Constant (mg^2/cm^4hr)	Total Specific Wt. Gain (mg/cm^2)
$Sm_2Si_2O_7$-Si_3N_4	14.0×10^{-4}*	0.644
$Gd_2Si_2O_7$-Si_3N_4	6.1×10^{-4}	0.346
$Y_2Si_2O_7$-Si_3N_4	5.1×10^{-4}	0.313
$Dy_2Si_2O_7$-Si_3N_4	5.0×10^{-4}	0.314
$Yb_2Si_2O_7$-Si_3N_4	3.7×10^{-4}	0.268
$Er_2Si_2O_7$-Si_3N_4	3.3×10^{-4}	0.252

* Determined for the period 72-192 hr (parabolic behavior)

Table 2. X-ray Diffraction of Oxidized Surfaces

Material	Major Phases	Minor Phases
$Y_2Si_2O_7$-Si_3N_4	β-$Y_2Si_2O_7$, SiO_2*	Si_2ON_2, β-Si_3N_4
$Sm_2Si_2O_7$-Si_3N_4	*A*-$Sm_2Si_2O_7$, SiO_2	Si_2ON_2, β-Si_3N_4
$Gd_2Si_2O_7$-Si_3N_4	δ-$Gd_2Si_2O_7$, SiO_2	Si_2ON_2, β-Si_3N_4
$Dy_2Si_2O_7$-Si_3N_4	δ-$Dy_2Si_2O_7$, SiO_2	α-$Dy_2Si_2O_7$, Si_2ON_2, β-Si_3N_4
$Er_2Si_2O_7$-Si_3N_4	β-$Er_2Si_2O_7$, SiO_2	Si_2ON_2, β-Si_3N_4
$Yb_2Si_2O_7$-Si_3N_4	β-$Yb_2Si_2O_7$, SiO_2	Si_2ON_2, β-Si_3N_4

* as α-cristobalite

Figure Captions

Figure 1. Plot of specific weight gain as a function of time, at 1400°C.

Figure 2. Parabolic plot of specific weight gain as a function of time, at 1400°C.

Figure 3. Scanning electron micrographs of the oxidized surfaces imaged using secondary electrons, showing surface topography and morphology and preference in direction of disilicate growth.

Figure 4. Scanning electron micrographs of the oxidized surfaces imaged using backscattered electrons to obtain compositional contrast. Darkest-contrast phase is cristobalite, medium-contrast phase is residual silicate, and brightest-contrast phase is the rare-earth disilicate.

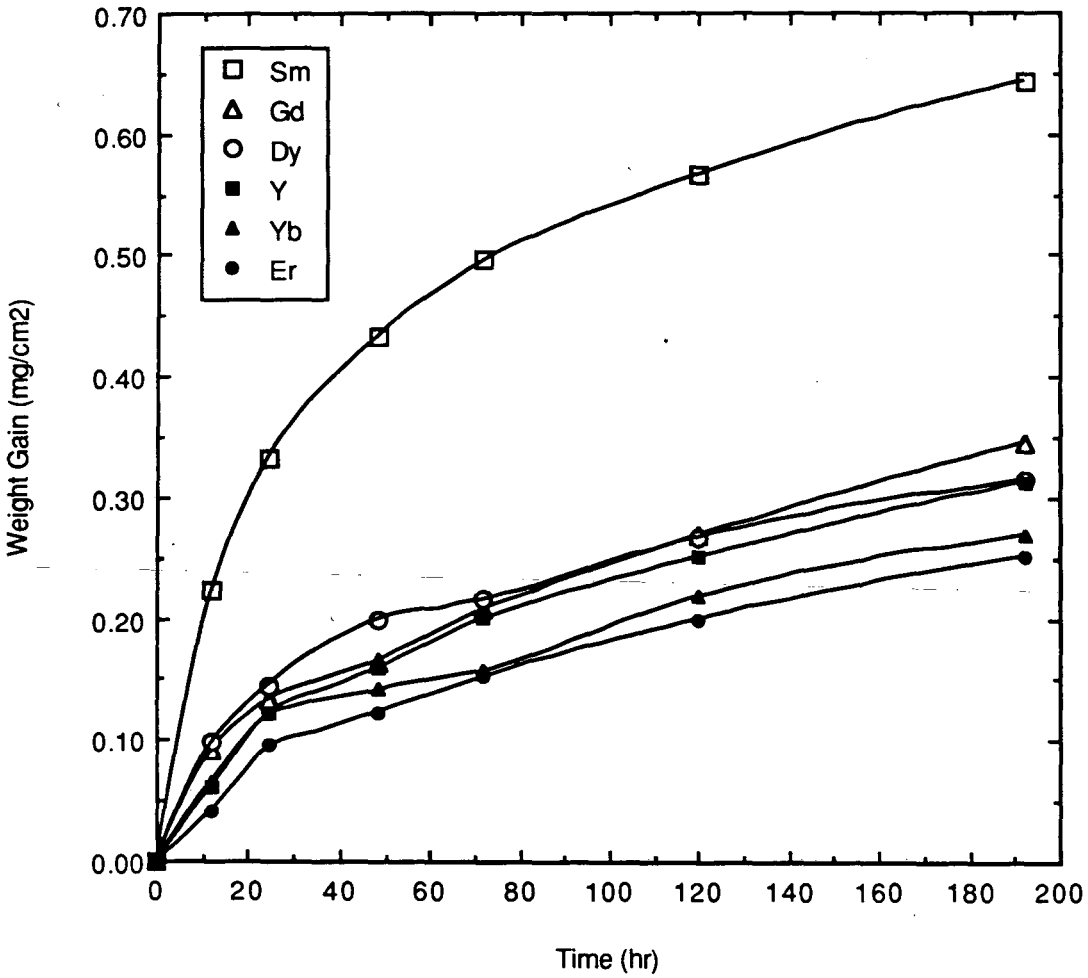
0.70
0.60
0.50
0.40
0.30
0.20
0.10
0.00
Weight Gain (mg/cm2)
Sm
Gd
Dy
Y
Yb
Er
0
20
40
60
80
100
120
140
160
180
200
Time (hr)
XBL 916-1287

Figure 1

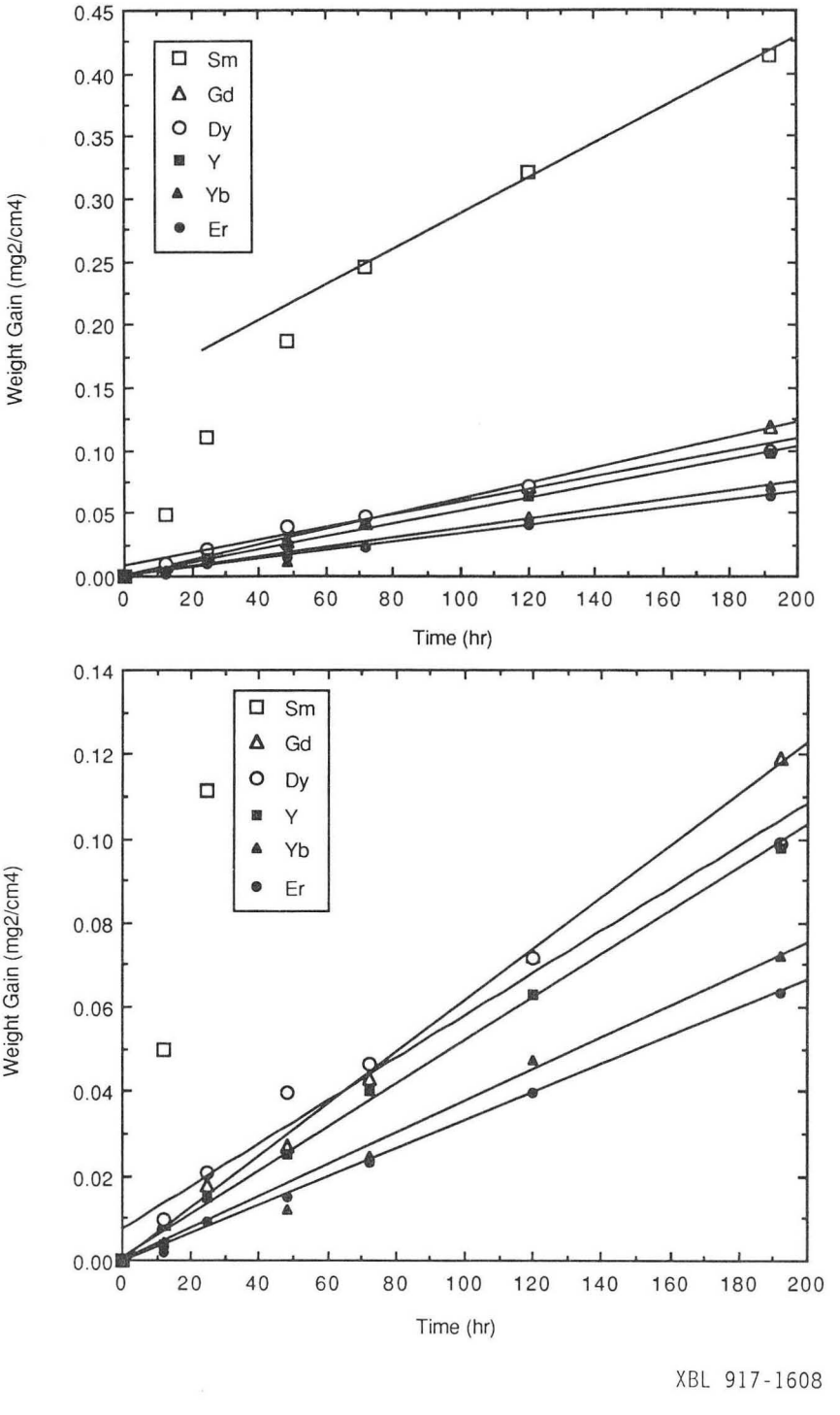
Sm
Gd
Dy
Y
Yb
Er
Weight Gain (mg2/cm4)
Time (hr)
0.45
0.40
0.35
0.30
0.25
0.20
0.15
0.10
0.05
0.00
0.14
0.12
0.10
0.08
0.06
0.04
0.02
0.00
0 20 40 60 80 100 120 140 160 180 200
XBL 917-1608

Figure 2

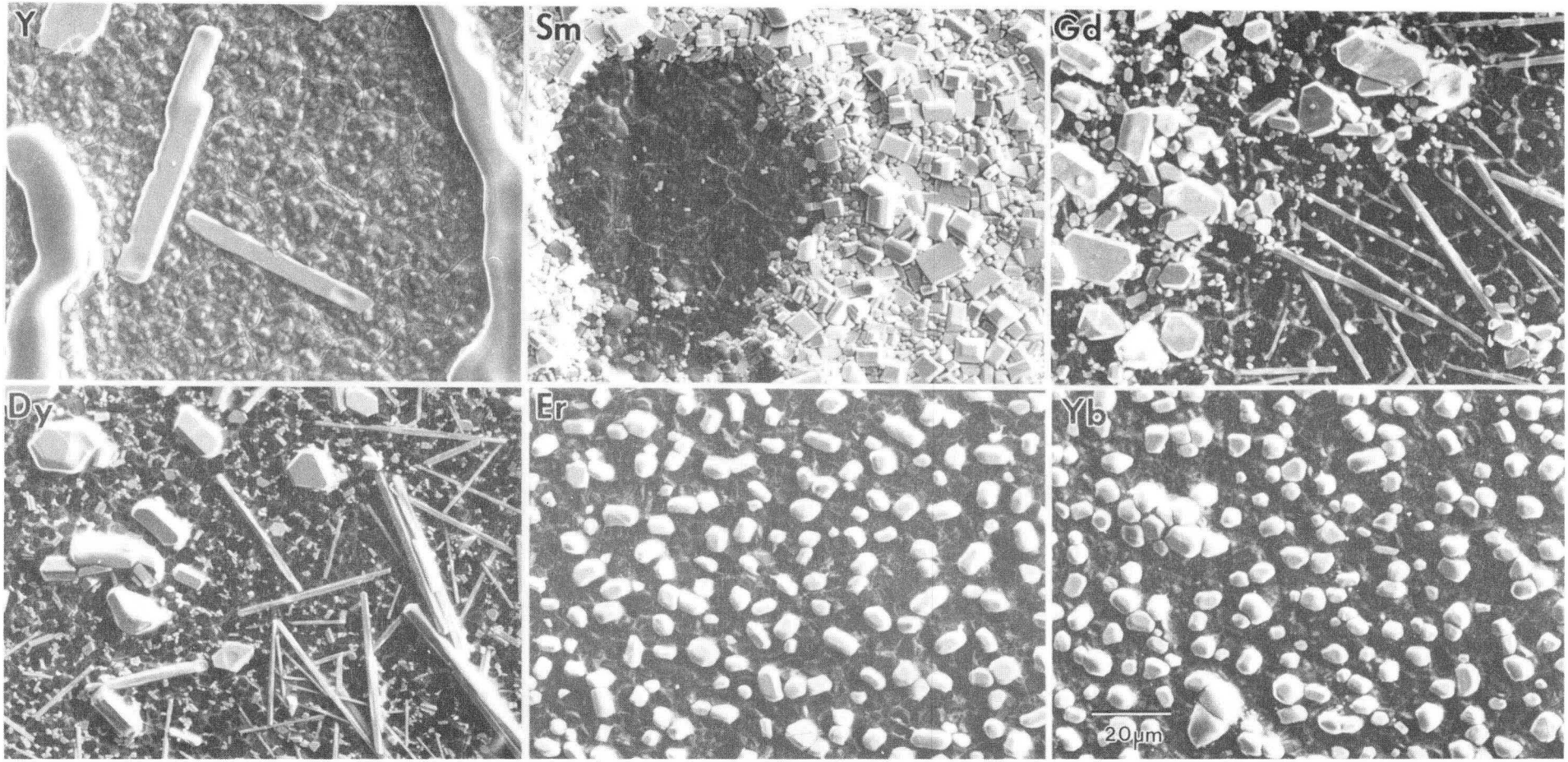

XBB 913-1898

Figure 3

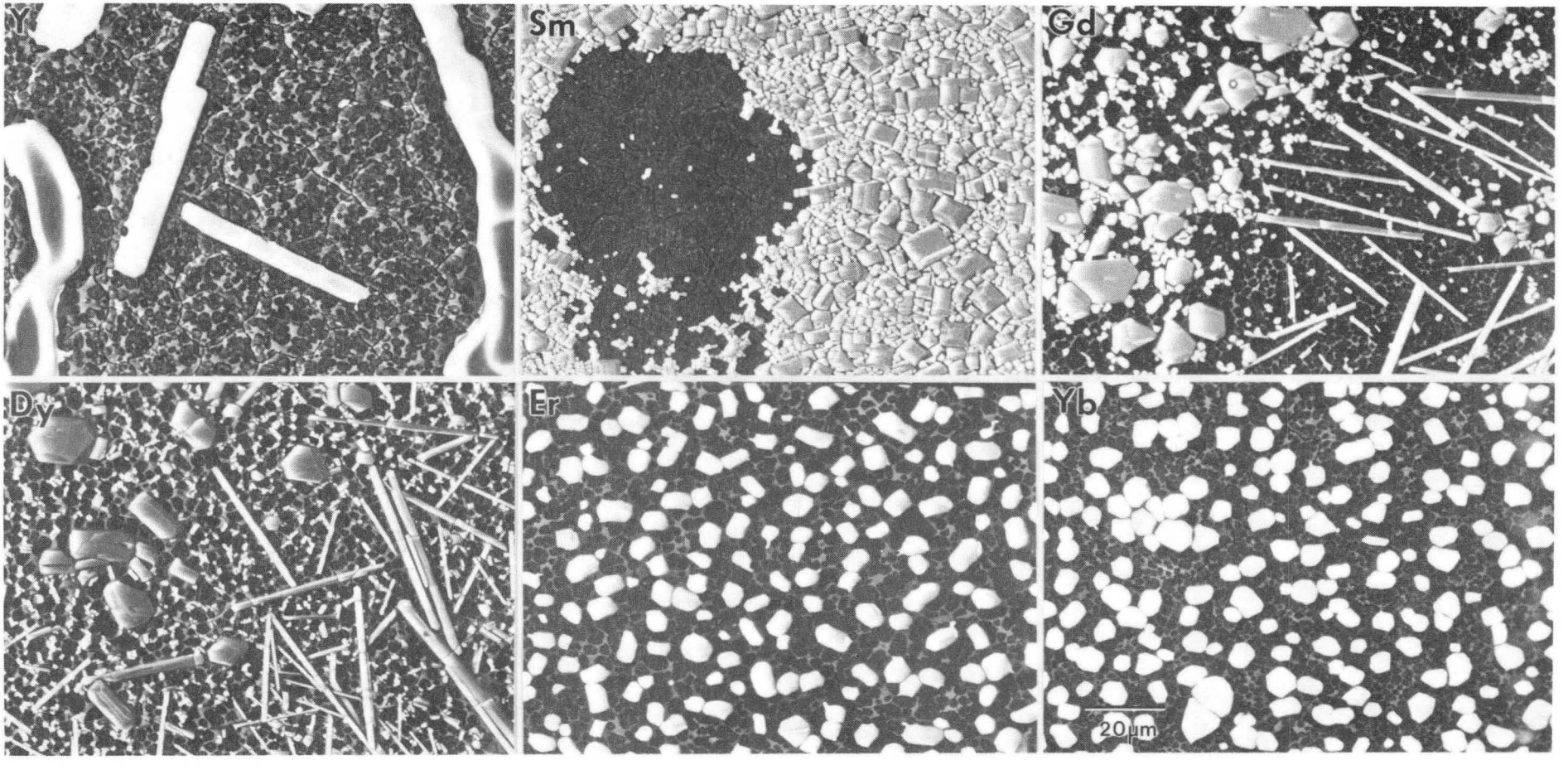

XBB 913-1897

Figure 4

LAWRENCE BERKELEY LABORATORY
UNIVERSITY OF CALIFORNIA
INFORMATION RESOURCES DEPARTMENT
BERKELEY, CALIFORNIA 94720